

# Active vibration robust control for FGM beams with piezoelectric layers

Yalan Xu\*, Zhouli Li and Kongming Guo

School of Electronic & Mechanical Engineering, Xidian University, Xi'an 710071, PR China

(Received September 29, 2017, Revised April 11, 2018, Accepted April 18, 2018)

**Abstract.** The dynamic output-feedback robust control method based on linear matrix inequality (LMI) method is presented for suppressing vibration response of a functionally graded material (FGM) beam with piezoelectric actuator/sensor layers in this paper. Based on the reduced model obtained by using direct mode truncation, the linear fractional state space representation of a piezoelectric FGM beam with material properties varying through the thickness is developed by considering both the inherent uncertainties in constitution material properties as well as material distribution and the model error due to mode truncation. The dynamic output-feedback robust H-infinity control law is implemented to suppress the vibration response of the piezoelectric FGM beam and the LMI method is utilized to convert control problem into convex optimization problem for efficient computation. In numerical studies, the flexural vibration control of a cantilever piezoelectric FGM beam is considered to investigate the accuracy and efficiency of the proposed control method. Compared with the efficient linear quadratic regulator (LQR) widely employed in literatures, the proposed robust control method requires less control voltage applied to the piezoelectric actuator in the case of same control performance for the controlled closed-loop system.

**Keywords:** FGM; piezoelectric layers; dynamic output-feedback robust control; linear matrix inequality; uncertainty

## 1. Introduction

As a special class of composite material, functionally graded materials (FGMs) have received extensive attention, which are fabricated from two or more phases of material constituents with continuously gradual changing material properties and possess resistant high temperature gradient and strong mechanical performance (Koizumi 1993). A great deal of research has already been reported on the static and thermo-elastic analysis (Swaminathan and Sangeetha 2017, Nie *et al.* 2013, Reddy *et al.* 2016), buckling analysis (Shen and Wang 2016) and dynamic analysis (Huang and Li 2010, Hemmatnezhad *et al.* 2013, Wang *et al.* 2016, Lee and Lee 2017) of structures made of FGMs over the past decades. On the other hand, the introduction of piezoelectric materials may form the intelligent FGM structures. In literatures, dynamic characteristics and responses of FGM structures with piezoelectric layers have been widely studied (Huang and Shen 2006, Ray and Sachade 2006, Bodaghi *et al.* 2014, Duc *et al.* 2015, Wu and Liu 2016).

With the further research on dynamics of FGM structures with piezoelectric layers, more and more attention has been focused on the investigation of the active vibration control for FGM structures integrated with piezoelectric actuators and sensors (Shirazi *et al.* 2011, Jadhav and Bajoria 2013, Kiani *et al.* 2013, Dogan 2014, Bruant and Proslie 2016, Selim *et al.* 2016, 2017, Nguyen-Quang *et al.* 2017), in which the constant-gain velocity feedback algorithm is mostly used. Jadhav and Bajoria

(2013) investigated the free and forced vibration analysis of piezoelectric FGM plate, and the structural vibration is suppressed by using a negative velocity feedback control law. Kiani *et al.* (2013) have discussed dynamic analysis and active control of shallow doubly curved piezoelectric FGM panels in which the dynamic equation has been developed by using the modified Sander's shell theory, and the vibration was suppressed by using the classical negative velocity feedback control method. Dogan (2014) has discussed the active control of the nonlinear vibration of the functionally graded material plate under random excitation by using a velocity feedback control technique. Selim *et al.* (2016, 2017) have investigated the active vibration control of FGM plates and carbon nanotube reinforced composite (CNTRC) plates, respectively, in which a novel element-free IMLS-Ritz model is developed for studying the free vibration behavior and a constant velocity feedback approach is adopted for the active vibration control of structures.

Besides, the optimal control was applied to the active control of FGM structures in order to improve the control performance. Bruant and Proslie (2013) have investigated active vibration control of a piezoelectric FGM beam by using the linear quadratic regulator (LQR) control law. As a kind of static state-feedback optimal control scheme, the knowledge of the state variables is needed in the vibration control. However, it is not easy to capture complete variables by using sensors and a state observer is essential in LQR method which may require numerous computations (Rittenschober and Schlacher 2012). In order to avoid using the state observer and improve the control performance, an attempt to seek a dynamic output-feedback controller (Valter *et al.* 2015, Chang *et al.* 2016, Wei and Park 2017) will be made in this paper.

\*Corresponding author, Associate Professor  
E-mail: [xyalan@hotmail.com](mailto:xyalan@hotmail.com)

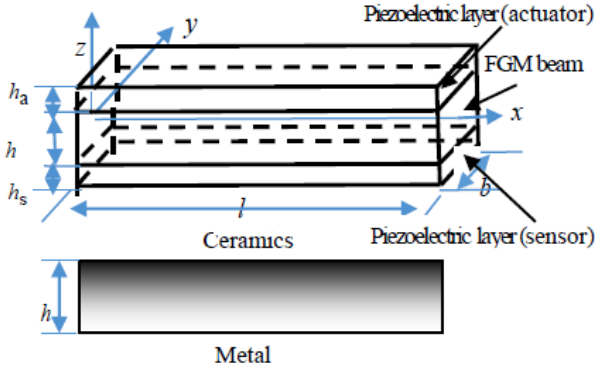


Fig. 1 Configuration of piezoelectric FGM beam

Owing to the reason that the design of model-based dynamic controller requires the accurate modeling of the open-loop system, the uncertainties in FGM structures should be considered in the stage of control design in order to guarantee the robustness of the closed-loop system. First, the uncertainties in constitution material properties and volume fraction index for FGMS are inevitable due to the complexity in the manufacturing and fabrication process of FGMS, which will be reflected on the uncertainties in structural dynamic characteristics and dynamic responses. In literatures, the influences of the uncertainties in material properties and volume fraction index for FGMS on the system dynamics have been widely reported (Lal 2007, Shaker 2008, Shegokar and Lal 2014, Mahammad and Singh 2015, Xu *et al.* 2015, 2016). Furthermore, modeling uncertainty may result from the model reduction which is required for obtaining the implementable relatively low-order controller. In model-reduction approaches, the direct mode truncation is commonly used to obtain a relatively low-order model including dominating low-frequency modes. In the active control, un-modeled high-frequency modes may lead to the instability of the closed-loop system (Xu *et al.* 2015). To the best of the author's knowledge, few studies have investigated robust control methods of FGM structures with considering uncertainties mentioned above. In this paper, based on the linear fractional state space model of piezoelectric FGM beams considering the uncertainties in both modal parameters and modeling, a dynamic output-feedback robust controller is designed by using linear matrix inequality (LMI) method (Reza and Esfanjani 2016, Li and Adeli 2016, Berardengo 2017) in order to suppress the vibration response due to the disturbance, and the corresponding comparative studies are conducted.

## 2. Configuration of piezoelectric FGM beam

An FGM beam with bonded piezoelectric layers as sensors and actuators having the length  $l$ , width  $b$ , thickness  $h$  of host FGM beam and thickness  $h_a/h_s$  of piezoelectric actuator/sensor with co-ordinate system  $(oxyz)$  as shown in Fig. 1.

The top layer of the laminated beam is the piezoelectric actuator layer and the bottom layer is the piezoelectric

sensor layer. The intermediate layer is an FGM beam made of the combined metal and ceramics, its properties are graded through the thickness direction according to the following volume fraction power law distribution (Segokar and Lal 2014)

$$P_F(z) = (P_T - P_B) \left( \frac{2z+h}{2h} \right)^n + P_B, \quad (1)$$

$$-\frac{h}{2} \leq z \leq \frac{h}{2}, \quad 0 \leq n < \infty$$

where  $P_F$  denotes the effective material property (e.g., elastic modulus, mass density) of the host FGM,  $P_T$ ,  $P_B$  denote the material properties of the top surface and bottom surface material of host FGM beam, respectively.  $n$  denotes the volume fraction index.

## 3. Dynamics modeling and model reduction

### 3.1 Theory formulation for host FGM beam

The displacement field described by the third-order shear deformation theory (TSDT) of Reddy can be given as

$$\mathbf{u} = \begin{Bmatrix} u(x, z, t) \\ w(x, t) \end{Bmatrix} = \begin{Bmatrix} u_0(x, t) + z\phi_x(x, t) - c_1 z^3 \left( \phi_x(x, t) + \frac{\partial w_0(x, t)}{\partial x} \right) \\ w_0(x, t) \end{Bmatrix} \quad (2)$$

where  $u_0(x, t)$ ,  $w_0(x, t)$  are the axial and transverse displacements of the mid-plane in the  $x, z$  directions, respectively,  $\phi_x$  is the cross-sectional rotation, and

$$c_1 = \frac{4}{3h^2}.$$

The strain field in the case of the small deformation can be written as

$$\boldsymbol{\varepsilon} = \begin{Bmatrix} \varepsilon_x \\ \gamma_{xz} \end{Bmatrix} = \begin{Bmatrix} \frac{\partial u_0}{\partial x} + z \frac{\partial \phi_x}{\partial x} - c_1 z^3 \left( \frac{\partial \phi_x}{\partial x} + \frac{\partial^2 w_0}{\partial x^2} \right) \\ \phi_x + \frac{\partial w_0}{\partial x} - 3c_1 z^2 \left( \phi_x + \frac{\partial w_0}{\partial x} \right) \end{Bmatrix} \quad (3)$$

The stress field is given as

$$\boldsymbol{\sigma} = \begin{Bmatrix} \sigma_x \\ \tau_{xz} \end{Bmatrix} = \mathbf{D}_F \begin{Bmatrix} \varepsilon_x \\ \gamma_{xz} \end{Bmatrix}, \quad \mathbf{D}_F = \begin{bmatrix} \frac{E_F(z)}{1-\nu^2} & 0 \\ 0 & \frac{E_F(z)}{2(1+\nu)} \end{bmatrix} \quad (4)$$

where  $E_F(z)$  is the effective Young's modulus, which is the function of  $z$  for the FGM beam, and the Poisson's ratio  $\nu$  is assumed to be constant.

### 3.2 Piezoelectric constitute equation

For one-dimensional structures, the constitutive relationship of piezoelectric material coupling elastic and electric field is given by (Duc *et al.* 2015)

$$\mathbf{D}_z = \boldsymbol{\varepsilon} \boldsymbol{\varepsilon} + \Xi_{33}^E \mathbf{E}_z, \quad \boldsymbol{\sigma} = \mathbf{S}^E \boldsymbol{\varepsilon} - \mathbf{e}^T \mathbf{E}_z \quad (5)$$

where  $\mathbf{D}_z$ ,  $\mathbf{E}_z$  denote electric field and electric displacement in the  $z$  direction,  $\boldsymbol{\sigma}$ ,  $\boldsymbol{\varepsilon}$  are stress and strain vector, respectively.  $\mathbf{e}$ ,  $\mathbf{S}^E$ ,  $\Xi_{33}^E$  are the piezoelectric constant matrix, material elastic constant matrix and dielectric coefficient, respectively.

### 3.3 Finite element model

The displacements ( $u_0$   $w_0$   $\frac{\partial w_0}{\partial x}$   $\phi_0$   $\Phi$ ) at the mid-plane and electric potential for a beam element can be defined in terms of nodal variables as follows

$$\left\{ u_0 \quad w_0 \quad \frac{\partial w_0}{\partial x} \quad \phi_x \right\}^T = \mathbf{N} \mathbf{q}^e, \quad \left\{ \Phi_p \right\} = \mathbf{N}_\Phi \Phi_p^e \quad (6)$$

where  $\mathbf{q}^e$ ,  $\Phi_p^e$  are the generalized nodal displacements and the nodal electric potentials respectively.  $\mathbf{N}$ ,  $\mathbf{N}_\Phi$  are the shape function matrix. So, the displacement field can be written as

$$\begin{aligned} \begin{Bmatrix} u \\ w \end{Bmatrix} &= \begin{bmatrix} \mathbf{N}_u \\ \mathbf{N}_w \end{bmatrix} \mathbf{q}^e, \\ \mathbf{N}_u &= \begin{bmatrix} 1 & 0 & -c_1 z^3 & z - c_1 z^3 \end{bmatrix} \mathbf{N}, \\ \mathbf{N}_w &= \begin{bmatrix} 0 & 1 & 0 & 0 \end{bmatrix} \mathbf{N} \end{aligned} \quad (7)$$

The stress field can be expressed in terms of nodal variables as follows

$$\begin{aligned} \boldsymbol{\varepsilon} &= \mathbf{B}_u \mathbf{q}^e, \quad \mathbf{B}_u = \begin{bmatrix} \mathbf{B}_\varepsilon \\ \mathbf{B}_\gamma \end{bmatrix}, \\ \mathbf{B}_\varepsilon &= \begin{bmatrix} 1 & 0 & -c_1 z^3 & z - c_1 z^3 \end{bmatrix} \frac{\partial \mathbf{N}}{\partial x}, \\ \mathbf{B}_\gamma &= \begin{bmatrix} 0 & 0 & 1 - 3c_1 z^2 & 1 - 3c_1 z^2 \end{bmatrix} \mathbf{N} \end{aligned} \quad (8)$$

The electric field can be expressed in terms of nodal electric potentials.

$$\mathbf{E}_z = -\nabla \Phi_p = -\mathbf{B}_\Phi \Phi_p, \quad \mathbf{B}_\Phi = \nabla \mathbf{N}_\Phi \quad (9)$$

The kinetic energy for FGM beam with piezoelectric layers can be expressed as

$$T = \frac{1}{2} \int_{V_F^e} \rho_F(z) (\dot{u}^2 + \dot{w}^2) dV + \frac{1}{2} \int_{V_a^e + V_s^e} \rho_p (\dot{u}^2 + \dot{w}^2) dV \quad (10)$$

where  $\rho_F(z)$  is the effective mass density, which is the function of  $z$  for the FGM beam, and  $\rho_p$  is the mass density of piezoelectric material.

The strain energy for FGM beam with piezoelectric layers can be expressed as

$$\begin{aligned} U &= \frac{1}{2} \int_{V_F^e} \boldsymbol{\varepsilon}^T \mathbf{D}_F \boldsymbol{\varepsilon} dV + \frac{1}{2} \int_{V_a^e} \boldsymbol{\varepsilon}^T (\mathbf{S}^E \boldsymbol{\varepsilon} - \mathbf{e}^T \mathbf{B}_\Phi \Phi_a^e) dV \\ &\quad + \frac{1}{2} \int_{V_s^e} \boldsymbol{\varepsilon}^T (\mathbf{S}^E \boldsymbol{\varepsilon} - \mathbf{e}^T \mathbf{B}_\Phi \Phi_s^e) dV \\ &\quad + \frac{1}{2} \int_{V_a^e} \Phi_a^{eT} \mathbf{B}_\Phi^T (\boldsymbol{\varepsilon} \boldsymbol{\varepsilon} - \Xi_{33}^E \mathbf{B}_\Phi \Phi_a^e) dV \\ &\quad - \frac{1}{2} \int_{V_s^e} \Phi_s^{eT} \mathbf{B}_\Phi^T (\boldsymbol{\varepsilon} \boldsymbol{\varepsilon} - \Xi_{33}^E \mathbf{B}_\Phi \Phi_s^e) dV \end{aligned} \quad (11)$$

The external work is given as

$$W^e = \mathbf{F}_f^{eT}(t) \mathbf{q}^e - \int_{A^e} \xi_0 \left( \mathbf{B}_\Phi \Phi_a^{eT} \Phi_a^e + \mathbf{B}_\Phi \Phi_s^{eT} \Phi_s^e \right) dA \quad (12)$$

where  $\xi_0$  is the absolute dielectric constant of piezoelectric material.

Substituting Eq. (6)-Eq. (9) into Eq. (10)-Eq. (11) and applying Hamilton's principle, the following finite element equation of free vibration for the  $e$ th element can be obtained

$$\begin{aligned} \mathbf{M}^e \ddot{\mathbf{q}}^e(t) + (\mathbf{K}_F^e + \mathbf{K}_p^e) \dot{\mathbf{q}}^e(t) - \mathbf{K}_{Fa}^e \Phi_a^e(t) - \mathbf{K}_{Fs}^e \Phi_s^e(t) &= \mathbf{F}_f^e(t), \\ \mathbf{K}_{aF}^e \mathbf{q}^e(t) + \mathbf{K}_{aa}^e \Phi_a^e(t) &= - \int_{A^e} \frac{\xi_0}{h_a} \mathbf{B}_\Phi dxdy, \\ \mathbf{K}_{sF}^e \mathbf{q}^e(t) + \mathbf{K}_{ss}^e \Phi_s^e(t) &= 0 \end{aligned} \quad (13)$$

where the matrices  $\mathbf{M}^e$ ,  $\mathbf{K}_F^e$ ,  $\mathbf{K}_p^e$ ,  $\mathbf{K}_{Fa}^e$ ,  $\mathbf{K}_{Fs}^e$ ,  $\mathbf{K}_{aF}^e$ ,  $\mathbf{K}_{aa}^e$ ,  $\mathbf{K}_{ss}^e$  are given by

$$\begin{aligned} \mathbf{M}^e &= \int_{V_F^e} \rho_F(z) (\mathbf{N}_u^T \mathbf{N}_u + \mathbf{N}_w^T \mathbf{N}_w) dV \\ &\quad + \int_{V_a^e + V_s^e} \rho_p (\mathbf{N}_u^T \mathbf{N}_u + \mathbf{N}_w^T \mathbf{N}_w) dV, \\ \mathbf{K}_F^e &= \int_{V_F^e} \mathbf{B}_u^T \mathbf{D}_F \mathbf{B}_u dV, \quad \mathbf{K}_p^e = \int_{V_a^e + V_s^e} \mathbf{B}_u^T \mathbf{S}^E \mathbf{B}_u dV, \\ \mathbf{K}_{Fa}^e &= \mathbf{K}_{aF}^e = \int_{V_a^e} \mathbf{B}_u^T \mathbf{e}^T \mathbf{B}_\Phi dV, \quad \mathbf{K}_{Fs}^e = \mathbf{K}_{sF}^e = \int_{V_s^e} \mathbf{B}_u^T \mathbf{e}^T \mathbf{B}_\Phi dV, \\ \mathbf{K}_{aa}^e &= \int_{V_a^e} \mathbf{B}_\Phi^T \mathbf{e}^T \mathbf{B}_\Phi dV, \quad \mathbf{K}_{ss}^e = \int_{V_s^e} \mathbf{B}_\Phi^T \mathbf{e}^T \mathbf{B}_\Phi dV \end{aligned} \quad (14)$$

Further, we obtain the following dynamic vibration equation in the case that there is no voltage applied to the piezoelectric sensor layer

$$\begin{aligned} \mathbf{M}^e \ddot{\mathbf{q}}^e(t) + \mathbf{K}^e \mathbf{q}^e(t) &= \mathbf{F}_f^e(t) - \mathbf{F}_{\text{control}}^e(t) \\ &= \mathbf{G}_f^e \mathbf{f}(t) - \mathbf{Q}_{\text{control}}^e \Phi_a^e(t) \end{aligned} \quad (15)$$

where the matrices  $\mathbf{K}^e$ ,  $\mathbf{G}_f^e(t)$ ,  $\mathbf{Q}_{\text{control}}^e(t)$  are given by

$$\begin{aligned}\mathbf{K}^e &= \mathbf{K}_F^e + \mathbf{K}_p^e + \mathbf{K}_{Fa}^e \mathbf{K}_{aa}^{-1} \mathbf{K}_{aF}^e + \mathbf{K}_{Fs}^e \mathbf{K}_{ss}^{-1} \mathbf{K}_{sF}^e, \\ \mathbf{G}_f^e(t) &= \iint_{A^e} \mathbf{N}^T dx dy, \\ \mathbf{Q}_{\text{control}}^e(t) &= \mathbf{K}_{Fa} \mathbf{K}_{aa}^{-1} \iint_{A^e} \xi_0 / h_a dx dy\end{aligned}\quad (16)$$

For the sensor layer, the applied charge is zero and the converse piezoelectric effect is assumed negligible. Thus, the sensor voltage is obtained by (Pota and Alberts 1995)

$$v_s^e(t) = \mathbf{Q}_{\text{out}}^e \mathbf{q}^e(t), \quad \mathbf{Q}_{\text{out}}^e = \frac{h_s(h + h_s)}{2A^e \Xi_{33}^E} \int \mathbf{e} \mathbf{B}_u dV \quad (17)$$

Assembling element equations and introducing the proportional damping matrix  $\mathbf{C}$ , we have

$$\begin{aligned}\mathbf{M}\ddot{\mathbf{q}}(t) + \mathbf{C}\dot{\mathbf{q}}(t) + \mathbf{K}\mathbf{q}(t) &= \mathbf{G}_f \mathbf{f}(t) - \mathbf{Q}_{\text{control}} \Phi_a(t), \\ \mathbf{v}_s(t) &= \mathbf{Q}_{\text{out}} \mathbf{q}^e(t)\end{aligned}\quad (18)$$

where  $\mathbf{C} = a\mathbf{K} + b\mathbf{M}$ ,  $a$  and  $b$  are Rayleigh coefficients.

### 3.4 Modal decoupling and model reduction

The  $j$ th modal frequency  $\omega_j$  and normalized mode shape  $\phi_j$  are governed by

$$(\mathbf{K} - \omega_j^2 \mathbf{M}) \phi_j = 0, \quad j = 1, 2, \dots, n \quad (19)$$

and making  $\mathbf{q}(t) = \boldsymbol{\mu} \boldsymbol{\eta}(t)$  by the normalized mode shape matrix  $\boldsymbol{\mu} = [\phi_1 \quad \phi_2 \quad \dots \quad \phi_n]$ , we have

$$\ddot{\boldsymbol{\eta}}(t) + \Lambda(\boldsymbol{\zeta}, \boldsymbol{\omega}) \dot{\boldsymbol{\eta}}(t) + \lambda(\boldsymbol{\omega}) \boldsymbol{\eta}(t) = \boldsymbol{\mu}^T \mathbf{G}_f \mathbf{f}(t) + \boldsymbol{\mu}^T \mathbf{Q}_{\text{control}} \Phi_a(t) \quad (20)$$

where  $\boldsymbol{\eta}(t)$  is the modal displacement vector, and  $\boldsymbol{\zeta}, \boldsymbol{\omega}$  are modal damping and modal frequency.

With mode truncation method, the dynamic equation of structure can be written as

$$\begin{aligned}\ddot{\eta}_i(t) + 2\zeta_i \omega_i \dot{\eta}_i(t) + \omega_i^2 \eta_i(t) &= \sum_{k=1}^K b_{ik\_a} \Phi_{ak}(t) \\ &+ \sum_{l=1}^L \tilde{b}_{il\_f} f_l, \quad i = 1, 2, \dots, m\end{aligned}\quad (21)$$

where  $\Phi_{ak}(t)$  is the  $k$ th applied voltage,  $f_l$  is the  $l$ th disturbance, and  $b_{ik\_a}$ ,  $b_{il\_f}$  are the influence coefficients of the  $k$ th actuating patch and the  $l$ th disturbance on the  $i$ th mode, respectively.

With structural modes, the performance displacement outputs of system and the measured voltage outputs of sensor can be defined as

$$\begin{aligned}y_i(t) &= \sum_{j=1}^m c_{ij\_y} \eta_j(t), \quad i = 1, 2, \dots, q, \\ v_{si}(t) &= \sum_{j=1}^p c_{ij\_s} \eta_j(t), \quad j = 1, 2, \dots, p\end{aligned}\quad (22)$$

where  $y_i(t)$  is the  $i$ th performance output,  $v_{si}(t)$  is the  $i$ th measured voltage output, and  $c_{ij\_y}$ ,  $c_{ij\_s}$  are the influence coefficients of the  $j$ th mode on the  $i$ th performance output and the  $i$ th measured voltage output, respectively.

## 4. State-space representation of linear fractional model

Eqs. (21)-(22) can be rearranged as the following state space form

$$\begin{aligned}\dot{\mathbf{x}}(t) &= \mathbf{A}(\boldsymbol{\zeta}, \boldsymbol{\omega}) \mathbf{x}(t) + \mathbf{B}_a(\boldsymbol{\mu}) \Phi_a(t) + \mathbf{B}_f(\boldsymbol{\mu}) \mathbf{f}(t) \\ \mathbf{y}(t) &= \mathbf{C}_y(\boldsymbol{\mu}) \mathbf{x}(t) \\ \mathbf{v}_s(t) &= \mathbf{C}_s(\boldsymbol{\mu}) \mathbf{x}(t)\end{aligned}\quad (23)$$

where  $\mathbf{x}(t) = [\eta_1(t), \dot{\eta}_1(t), \eta_2(t), \dot{\eta}_2(t), \dots, \eta_m(t), \dot{\eta}_m(t)]^T$  is state vector and  $\Phi_a(t)$  is the control voltage input vector,  $\mathbf{f}(t)$  is the external disturbance input vector,  $\mathbf{y}(t)$  is the performance output of the system  $\mathbf{v}_s(t)$  is the measured voltage output of the sensor, and  $\mathbf{A}(\boldsymbol{\zeta}, \boldsymbol{\omega})$  is the system matrix which depends on the modal parameters as follows

$$\begin{aligned}\mathbf{A}(\boldsymbol{\zeta}, \boldsymbol{\omega}) &= \text{diag}\{\mathbf{A}_1, \dots, \mathbf{A}_i, \dots, \mathbf{A}_m\}, \\ \mathbf{A}_i(\zeta_i, \omega_i) &= \begin{bmatrix} 0 & 1 \\ -\omega_i^2 & -2\zeta_i \omega_i \end{bmatrix}\end{aligned}\quad (24)$$

The inherent uncertainties in constitution material properties and material distribution will lead to the random fluctuation of structural dynamic characteristics (Xu *et al.* 2015, 2016). The uncertainties in modal parameters are dealt as follows

$$\tilde{\omega}_i = \omega_i + \Delta_{\omega_i} \delta_{1i}, \quad \tilde{\zeta}_i = \zeta_i + \Delta_{\zeta_i} \delta_{2i} \quad (25)$$

where  $\omega_i$ ,  $\zeta_i$  are the nominal value of modal parameters,  $\Delta_{\omega_i}$ ,  $\Delta_{\zeta_i}$  are the ranges of fluctuation of uncertain modal parameters around the nominal values  $\omega_i$ ,  $\zeta_i$ , and  $\delta_{1i}$ ,  $\delta_{2i}$  are the normalized uncertain parameters for modal parameters with the bound norms  $\|\delta_{1i}\| \leq 1$  and  $\|\delta_{2i}\| \leq 1$ .

As such, with the uncertain modal parameters  $\tilde{\boldsymbol{\omega}}, \tilde{\boldsymbol{\zeta}}$ , the system matrix  $\mathbf{A}(\boldsymbol{\omega}, \boldsymbol{\zeta})$  can be developed as uncertain matrix  $\tilde{\mathbf{A}}(\tilde{\boldsymbol{\omega}}, \tilde{\boldsymbol{\zeta}})$  and its block  $\hat{\mathbf{A}}_i(\tilde{\omega}_i, \tilde{\zeta}_i)$  can be written as

$$\begin{aligned}\hat{\mathbf{A}}_i(\tilde{\omega}_i, \tilde{\zeta}_i) &= \begin{bmatrix} 0 & 1 \\ -\tilde{\omega}_i^2 & -2\tilde{\zeta}_i \tilde{\omega}_i \end{bmatrix} \\ &= \begin{bmatrix} 0 & 1 \\ -\omega_i^2 + 2\omega_i \Delta_{\omega_i} + \Delta_{\omega_i}^2 \delta_{1i}^2 & -2\zeta_i \omega_i - 2\zeta_i \omega_i \delta_{1i} - 2\omega_i \Delta_{\zeta_i} \delta_{2i} - 2\Delta_{\zeta_i \Delta_i} \Delta_{\omega_i} \delta_{1i} \delta_{2i} \end{bmatrix} \\ &= \mathbf{A}_i(\omega_i, \zeta_i) + \mathbf{E}_i(\Delta_{\omega_i}, \Delta_{\zeta_i}) \boldsymbol{\delta}_i \mathbf{F}_i(\omega_i, \zeta_i)\end{aligned}\quad (26)$$

where the matrices concerning the uncertainties can be given by

$$\mathbf{E}_i(\Delta\omega_i, \Delta\zeta_i) = \begin{bmatrix} 0 & 0 \\ -\Delta\omega_i & -\Delta\zeta_i \end{bmatrix}, \quad (27)$$

$$\delta_i = \begin{bmatrix} \delta_{1i} & 0 \\ 0 & \delta_{2i} \end{bmatrix}, \quad \mathbf{F}_i(\omega_i, \zeta_i) = \begin{bmatrix} 2\omega_i & 2\zeta_i \\ 0 & 2\omega_i \end{bmatrix}$$

Recalling Eq. (23), the state-space representation of the linear fractional model for the FGM structure with considering the uncertainties in modal parameters

$$\begin{aligned} \dot{\mathbf{x}}(t) &= \mathbf{A}(\boldsymbol{\omega}, \boldsymbol{\zeta})\mathbf{x}(t) + \mathbf{B}_a(\boldsymbol{\mu})\boldsymbol{\Phi}_a(t) \\ &\quad + \mathbf{B}_f(\boldsymbol{\mu})\mathbf{f}(t) + \mathbf{E}(\Delta\omega, \Delta\zeta)\mathbf{g}_{u1}(t), \\ \mathbf{y}(t) &= \mathbf{C}_y(\boldsymbol{\mu})\mathbf{x}(t), \\ \mathbf{v}_s(t) &= \mathbf{C}_s(\boldsymbol{\mu})\mathbf{x}(t), \\ \mathbf{h}_{u1}(t) &= \mathbf{F}(\boldsymbol{\omega}, \boldsymbol{\zeta})\mathbf{x}(t), \quad \mathbf{g}_{u1}(t) = \delta\mathbf{h}_{u1}(t) \end{aligned} \quad (28)$$

where the matrices introduced by the uncertainties are given by

$$\begin{aligned} \mathbf{E}(\Delta\zeta, \Delta\omega) &= \text{diag}\{\mathbf{E}_1(\Delta\omega_1, \Delta\zeta_1), \dots, \mathbf{E}_m(\Delta\omega_m, \Delta\zeta_m)\}, \\ \delta &= \text{diag}\{\delta_1, \dots, \delta_m\}, \\ \mathbf{F}(\boldsymbol{\zeta}, \boldsymbol{\omega}) &= \text{diag}\{\mathbf{F}_1(\omega_1, \zeta_1), \dots, \mathbf{F}_m(\omega_m, \zeta_m)\} \end{aligned} \quad (29)$$

Introducing the model error due to mode truncation (Sana and Rao 2000), we have

$$\tilde{\mathbf{G}}(s) = \mathbf{G}(s) + \mathbf{e}(s)\boldsymbol{\chi} \quad (30)$$

where  $\mathbf{e}(s)$  has to form the upper bound of the un-modeled high-frequency modes, which can be represented as the following state space form

$$\begin{aligned} \dot{\mathbf{x}}_e(t) &= \mathbf{A}_e\mathbf{x}_e(t) + \mathbf{B}_e\boldsymbol{\Phi}_a(t) \\ \mathbf{e}(t) &= \mathbf{C}_e\mathbf{x}_e(t) + \mathbf{D}_e\boldsymbol{\Phi}_a(t) \end{aligned} \quad (31)$$

and  $\boldsymbol{\chi}$  is the normalized uncertainty with the bound norm  $\|\boldsymbol{\chi}\|_\infty \leq 1$ . As a result, the state-space representation of linear fraction model for the FGM structure can be further developed as

$$\begin{aligned} \dot{\mathbf{x}}_1(t) &= \mathbf{A}_1\mathbf{x}_1(t) + \mathbf{B}_{1_a}\boldsymbol{\Phi}_a(t) + \mathbf{B}_{1_f}\mathbf{f}(t) + \mathbf{E}_1\mathbf{g}_u(t), \\ \mathbf{y}_1(t) &= \mathbf{C}_{1_y}\mathbf{x}_1(t) + \mathbf{E}_{1_y}\mathbf{g}_u(t), \\ \mathbf{v}_{1_s}(t) &= \mathbf{C}_{1_s}\mathbf{x}_1(t) + \mathbf{E}_{1_s}\mathbf{g}_u(t), \\ \mathbf{h}_u(t) &= \mathbf{F}_1\mathbf{x}_1(t) + \mathbf{F}_2\boldsymbol{\Phi}_a(t), \quad \mathbf{g}_u(t) = \Delta\mathbf{h}_u(t) \end{aligned} \quad (32)$$

where the state variables  $\mathbf{x}_1(t) = \{\dot{\mathbf{x}}(t) \quad \dot{\mathbf{x}}_e(t)\}^T$  and the system matrix, the input matrices and the output matrices are given as

$$\begin{aligned} \mathbf{A}_1 &= \text{diag}\{\mathbf{A}, \mathbf{A}_e\}, \quad \mathbf{B}_{1_a} = [\mathbf{B}_a \quad \mathbf{B}_e], \\ \mathbf{B}_{1_f} &= [\mathbf{B}_f \quad \mathbf{0}], \quad \mathbf{C}_{1_a} = [\mathbf{C}_y \quad \mathbf{0}], \quad \mathbf{C}_{1_s} = [\mathbf{C}_s \quad \mathbf{0}] \end{aligned} \quad (33)$$

and the matrices concerning uncertainties are given as

$$\begin{aligned} \mathbf{E}_1 &= [\mathbf{E} \quad \mathbf{0}], \quad \mathbf{E}_{1_y} = [\mathbf{0} \quad \mathbf{E}_y], \quad \mathbf{E}_{1_s} = [\mathbf{0} \quad \mathbf{E}_s], \\ \mathbf{F}_1 &= \text{diag}\{\mathbf{F}, \mathbf{C}_e\}, \quad \mathbf{F}_2 = [\mathbf{0} \quad \mathbf{D}_e]^T, \quad \Delta = \text{diag}\{\delta, \boldsymbol{\chi}\} \end{aligned} \quad (34)$$

## 5. Controller design based on LMI approach

This part is aimed at designing a dynamic output-feedback controller as follows

$$\begin{aligned} \dot{\mathbf{x}}_c(t) &= \mathbf{A}_c\mathbf{x}_c(t) + \mathbf{B}_c\mathbf{v}_s(t) \\ \boldsymbol{\Phi}_a(t) &= \mathbf{C}_c\mathbf{x}_c(t) + \mathbf{D}_c\mathbf{v}_s(t) \end{aligned} \quad (35)$$

where  $\mathbf{x}_c(t)$  is the state vector of the controller;  $\mathbf{A}_c, \mathbf{B}_c, \mathbf{C}_c, \mathbf{D}_c$  are unknown parameters.

Applying Eq. (35) to Eq. (32), the closed-loop system can be described as

$$\begin{aligned} \dot{\mathbf{z}}(t) &= \mathbf{A}_{cl}\mathbf{z}(t) + \mathbf{B}_{cl}\mathbf{f}(t) + \mathbf{E}_{cl}\mathbf{g}_u(t) \\ \mathbf{y}(t) &= \mathbf{C}_{cl_y}\mathbf{z}(t) + \mathbf{E}_{cl_y}\mathbf{g}_u(t) \\ \mathbf{h}_u(t) &= \mathbf{F}_{cl_z}\mathbf{z}(t) + \mathbf{F}_{cl_g}\mathbf{g}_u(t) \\ \boldsymbol{\Phi}_a(t) &= \mathbf{C}_{cl_\phi}\mathbf{z}(t) + \mathbf{D}_{cl_\phi}\mathbf{g}_u(t) \\ \mathbf{g}_u(t) &= \Delta\mathbf{h}_u(t) \end{aligned} \quad (36)$$

where  $\mathbf{z}(t)$  is the augmented state vector denoted by  $\mathbf{z}(t) = \{\mathbf{x}_1(t), \mathbf{x}_c(t)\}^T$  and the augmented system matrix, input matrices and output matrices are described as follows respectively

$$\begin{aligned} \mathbf{A}_{cl} &= \begin{bmatrix} \mathbf{A} + \mathbf{B}_{1_a}\mathbf{D}_c\mathbf{C}_{1_s} & \mathbf{B}_{1_a}\mathbf{C}_c \\ \mathbf{B}_c\mathbf{C}_{1_s} & \mathbf{A}_c \end{bmatrix}, \quad \mathbf{B}_{cl} = \begin{bmatrix} \mathbf{B}_{1_f} \\ \mathbf{0} \end{bmatrix}, \\ \mathbf{C}_{cl_y} &= [\mathbf{C}_{1_y} \quad \mathbf{0}], \quad \mathbf{C}_{cl_\phi} = [\mathbf{D}_c\mathbf{C}_{1_s} \quad \mathbf{C}_c] \end{aligned} \quad (37)$$

and the augmented influence matrices related to the uncertainties are expressed as

$$\begin{aligned} \mathbf{E}_{cl} &= \begin{bmatrix} \mathbf{E}_1 + \mathbf{B}_{1_a}\mathbf{D}_c\mathbf{E}_{1_s} \\ \mathbf{B}_c\mathbf{E}_{1_s} \end{bmatrix}, \quad \mathbf{E}_{cl_y} = \mathbf{E}_{1_y}, \\ \mathbf{F}_{cl_z} &= [\mathbf{F}_1 + \mathbf{F}_2\mathbf{D}_c\mathbf{C}_{1_y}, \mathbf{F}_2\mathbf{C}_c], \\ \mathbf{F}_{cl_g} &= \mathbf{F}_2\mathbf{D}_c\mathbf{E}_{1_s}, \quad \mathbf{D}_{cl_s} = \mathbf{D}_c\mathbf{E}_{1_s} \end{aligned} \quad (38)$$

In order to suppress the vibration response as well as guarantee the system stability, the robust controller can be designed by setting an upper bound  $\alpha$  on the  $H$ -infinity norm from the external disturbance  $\mathbf{f}(t)$  to the system response  $\mathbf{y}(t)$  of Eq. (36) as follows

$$\begin{aligned} d(\mathbf{z}^T(t)\mathbf{P}\mathbf{z}(t))/dt + \mathbf{y}^T(t)\mathbf{y}(t) - \alpha^2\mathbf{f}^T(t)\mathbf{f}(t) &< 0, \\ \mathbf{P} = \mathbf{P}^T &> 0 \end{aligned} \quad (39)$$

in the case of the uncertainties

$$\mathbf{g}_u^T(t)\mathbf{g}_u(t) \leq \mathbf{h}_u^T(t)\mathbf{h}_u(t) \quad (40)$$

Substituting Eq. (36) into Eqs. (39)-(40), the controller design problem can be transformed into the solution of the following matrix inequality by using the S-Procedure method (Xu *et al.* 2015)

$$\begin{bmatrix} \mathbf{A}_{cl}^T\mathbf{P} + \mathbf{P}\mathbf{A}_{cl} + \mathbf{C}_{cl_y}^T\mathbf{C}_{cl_y} + \beta\mathbf{F}_{cl_z}^T\mathbf{F}_{cl_z} & \mathbf{P}\mathbf{E}_{cl} + \mathbf{C}_{cl_\phi}^T\mathbf{E}_{cl_y} + \beta\mathbf{F}_{cl_g}^T\mathbf{F}_{cl_g} & \mathbf{P}\mathbf{B}_{cl} \\ \mathbf{E}_{cl_y}^T\mathbf{P} + \mathbf{E}_{cl_y}^T\mathbf{C}_{cl_y} + \beta\mathbf{F}_{cl_z}^T\mathbf{F}_{cl_z} & \mathbf{E}_{cl_y}^T\mathbf{E}_{cl_y} + \beta\mathbf{F}_{cl_g}^T\mathbf{F}_{cl_g} - \beta\mathbf{I} & \mathbf{0} \\ \mathbf{B}_{cl}^T\mathbf{P} & \mathbf{0} & -\alpha^2\mathbf{I} \end{bmatrix} < 0, \quad \beta \geq 0 \quad (41)$$

Rearranging Eq. (41) and utilizing the Schur complement theorem, Eq. (41) can be transformed into the following equivalent matrix inequality by,

$$\begin{bmatrix} \mathbf{A}_{cl}^T \mathbf{P} + \mathbf{P} \mathbf{A}_{cl} & \mathbf{P} \mathbf{E}_{cl} & \mathbf{P} \mathbf{B}_{cl} & \mathbf{F}_{cl,z}^T & \mathbf{C}_{cl}^T \\ * & -\mathbf{I} & \mathbf{0} & \mathbf{F}_{cl,g}^T & \mathbf{E}_{cl,y}^T \\ * & * & -\alpha^2 \mathbf{I} & \mathbf{0} & \mathbf{0} \\ * & * & * & -\mathbf{I} & \mathbf{0} \\ * & * & * & * & -\mathbf{I} \end{bmatrix} < 0 \quad (42)$$

Conducting the following partitioning

$$\mathbf{P} = \begin{bmatrix} \mathbf{p}_1 & \mathbf{p}_2 \\ \mathbf{p}_2^T & \mathbf{p}_3 \end{bmatrix}, \quad \mathbf{P}^{-1} = \begin{bmatrix} \hat{\mathbf{p}}_1 & \hat{\mathbf{p}}_2 \\ \hat{\mathbf{p}}_2^T & \hat{\mathbf{p}}_3 \end{bmatrix}, \quad \hat{\mathbf{F}}_1 = \begin{bmatrix} \hat{\mathbf{p}}_1 & \mathbf{I} \\ \hat{\mathbf{p}}_2^T & \mathbf{0} \end{bmatrix} \quad (43)$$

and performing a congruence transformation with  $\text{diag}\{\hat{\mathbf{F}}_1, \mathbf{I}, \mathbf{I}, \mathbf{I}, \mathbf{I}\}$  on Eq. (42), the nonlinear matrix inequality Eq. (42) can be converted into the linear matrix inequality and the controller design problem can be converted into the following linear convex optimization problem

$$\begin{array}{l} \text{Min } \alpha \\ \text{Subject to} \\ \begin{bmatrix} \mathbf{A}_1 \hat{\mathbf{p}}_1 + \hat{\mathbf{p}}_1 \mathbf{A}_1^T + \mathbf{B}_{1,s} \mathbf{C}_1 + \mathbf{C}_1^T \mathbf{B}_{1,s}^T & \mathbf{A}_1 + \mathbf{B}_{1,s} \mathbf{D}_c \mathbf{C}_1 + \mathbf{A}_1^T & \mathbf{E}_1 + \mathbf{B}_{1,s} \mathbf{D}_c \mathbf{E}_{1,s} & \mathbf{B}_{1,f} & \hat{\mathbf{p}}_1 \mathbf{F}_1^T + \mathbf{C}_1^T \mathbf{F}_2^T & \hat{\mathbf{p}}_1 \mathbf{C}_{13}^T \\ * & \mathbf{A}_1^T \hat{\mathbf{p}}_1 + \hat{\mathbf{p}}_1 \mathbf{A}_1 + \mathbf{C}_{1,s}^T \mathbf{B}_{1,s} + \mathbf{B}_{1,s} \mathbf{C}_{1,s} & \mathbf{p}_1 \mathbf{E}_1 + \mathbf{B}_{1,s} \mathbf{E}_{1,s} & \mathbf{p}_1 \mathbf{B}_{1,f} & \mathbf{F}_1^T + \mathbf{C}_{1,s} \mathbf{D}_c^T \mathbf{F}_2^T & \mathbf{C}_{1,s}^T \\ * & * & -\mathbf{I} & \mathbf{0} & \mathbf{E}_{1,s}^T \mathbf{D}_c^T \mathbf{F}_2^T & \mathbf{E}_{1,s}^T \\ * & * & * & -\alpha^2 \mathbf{I} & \mathbf{0} & \mathbf{0} \\ * & * & * & * & -\mathbf{I} & \mathbf{0} \\ * & * & * & * & * & -\mathbf{I} \end{bmatrix} < 0, \quad (44) \\ \begin{bmatrix} \hat{\mathbf{p}}_1 & \mathbf{I} \\ \mathbf{I} & \hat{\mathbf{p}}_1 \end{bmatrix} > 0 \end{array}$$

The parameters  $\mathbf{A}_t, \mathbf{B}_t, \mathbf{C}_t, \mathbf{D}_c, \mathbf{p}_1, \hat{\mathbf{p}}_1$  can be obtained by solving the above optimization problem, the parameter  $\hat{\mathbf{p}}_2$  can be obtained by the singular value decomposition (SVD) of the matrix  $\mathbf{I} - \mathbf{p}_1 \hat{\mathbf{p}}_1$ , and the unknown parameters  $\mathbf{A}_c, \mathbf{B}_c, \mathbf{C}_c$  of controller Eq. (35) can be obtained by

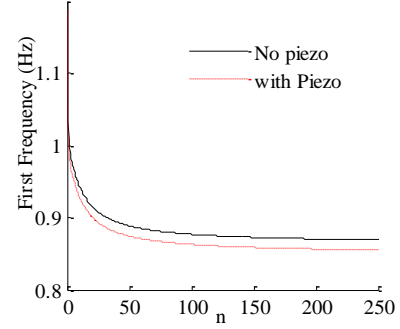
$$\begin{aligned} (\mathbf{U}, \mathbf{S}, \mathbf{V}) &= \text{SVD}(\mathbf{I} - \mathbf{p}_1 \hat{\mathbf{p}}_1), \quad \mathbf{p}_2 = \mathbf{V}, \quad \hat{\mathbf{p}}_2 = \mathbf{U} \mathbf{S}, \\ \mathbf{C}_c &= (\mathbf{C}_t - \mathbf{D}_c \mathbf{C}_{1,s} \hat{\mathbf{p}}_1)^{-1}, \\ \mathbf{B}_c &= \mathbf{p}_2^{-1} (\mathbf{B}_t - \mathbf{p}_1 \mathbf{B}_{1,a} \mathbf{D}_c), \\ \mathbf{A}_c &= \mathbf{p}_1^{-1} (\mathbf{A}_t - \mathbf{p}_1 (\mathbf{A}_1 + \mathbf{B}_{1,a} \mathbf{D}_c \mathbf{C}_{1,s}) \hat{\mathbf{p}}_1 \\ &\quad + \mathbf{p}_2 \mathbf{B}_c \mathbf{C}_{1,s} \hat{\mathbf{p}}_1 + \mathbf{p}_1 \mathbf{B}_{1,a} \mathbf{C}_c \hat{\mathbf{p}}_2^T) (\hat{\mathbf{p}}_2^T)^{-1} \end{aligned} \quad (45)$$

## 6. Simulation results

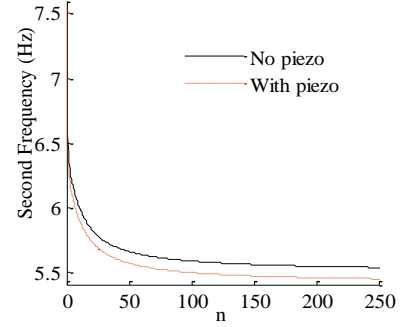
In this part, the flexural vibration control of a cantilever piezoelectric FGM beam with piezoelectric actuator bonded to the top surface and piezoelectric sensor bonded to the bottom surface is considered to investigate the effectiveness and efficiency of the proposed control method, in which the tip flexural vibration response will be suppressed by the proposed control method. The host FGM beam is composed of ceramics (Zirconia) and metal (Alumina) with the material properties of Young's elastic modulus  $E_c=151$  Gpa, mass density for Zirconia, and Young's elastic modulus

Table 1 First three modal frequencies  $f_i$  (Hz) for piezoelectric FGM beam

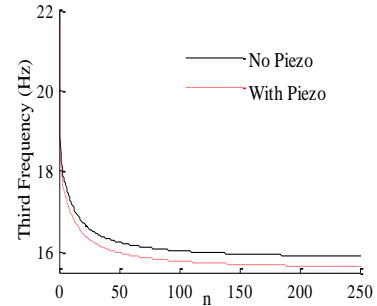
$f$	$\eta=0$		$\eta=05$		$\eta=5$		$\eta=50$		$\eta=90$	
	No piezo	With piezo	No piezo	With piezo	No piezo	With piezo	No piezo	With piezo	No piezo	With piezo
$i=1$	1.2045	1.1872	1.0830	1.0668	0.9691	0.9539	0.8886	0.8744	0.8634	0.8536
$i=2$	7.7784	7.5571	6.8957	6.7926	6.1674	6.0700	5.6564	5.5660	5.4965	5.4235
$i=3$	22.0312	21.7453	19.8189	19.5197	17.7106	17.4301	16.2580	15.9892	15.8923	15.6414



(a)



(b)



(c)

Fig. 2 Variations of modal frequencies with volume fraction index

$E_m=70$  Gpa, mass density  $\rho_m = 2707 \text{ kg/m}^3$  for Alumina. The Poisson's ratio is assumed to be constant 0.3 for each constituent material. In FGM, material properties are assumed to vary through the thickness according to power law distribution Eq. (1). For the piezoelectric layers, Young's elastic modulus, Poisson's ratio, mass density, piezoelectric constant, dielectric coefficient and absolute dielectric constant are  $E_p=2$  Gpa,  $\nu_p=0.3$ ,  $\rho_c=3000 \text{ kg/m}^3$ ,  $\rho_p=1800 \text{ kg/m}^3$ ,  $e_{31}=-1.062e-10 \text{ m/V}$ ,  $\epsilon_{33}^E = 1.5e-8 \text{ F/m}$ ,  $\zeta_0=0.0464 \text{ C/m}^2$ , respectively. The host FGM beam has the

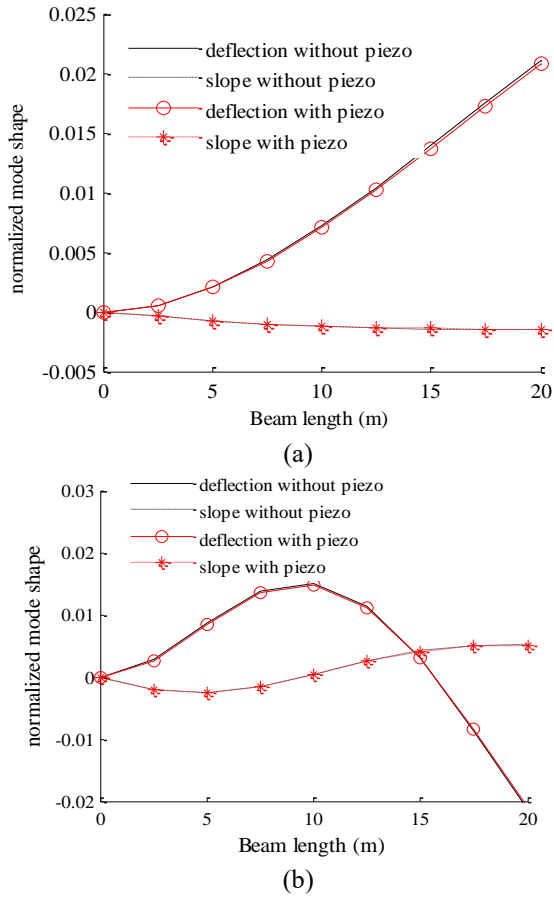


Fig. 3 First two mode shapes of piezoelectric FGM beam ( $n=2$ )

geometric parameters of 20 m in length, 0.4 m in thickness and 0.8 m in width, the piezoelectric layer has the same length and width as the host structure, and the thickness of piezoelectric layer is set to be 0.01 m in order not to have a great impact on the dynamic characteristics of the host beam. Eight elements are used to model the piezoelectric FGM beam in finite element simulation.

### 6.1 Dynamic characteristics

Firstly, Modal analysis is carried out to investigate the influence of piezoelectric layers on the dynamic characteristics of the structure. Compared to the FGM beam without piezoelectric layers, the first three modal frequencies of the piezoelectric FGM beam with the top piezoelectric layers as actuator and the bottom piezoelectric layer as sensor are list in Table 1 and the variations of modal frequencies with the volume fraction index  $n$  are shown in Fig. 2(a)-2(c).

From Table 1, the modal frequencies are slightly decreased with the introduction of the piezoelectric layers in the active control of FGM beam. It can be observed from Fig. 2 that the modal frequencies decrease with the increase of volume fraction index  $n$ . It is because the increase in volume fraction index leads to the increase in the volume of metal, and, as a result, the stiffness of FGM beam reduces. It is worth noting that modal frequencies nearly remain

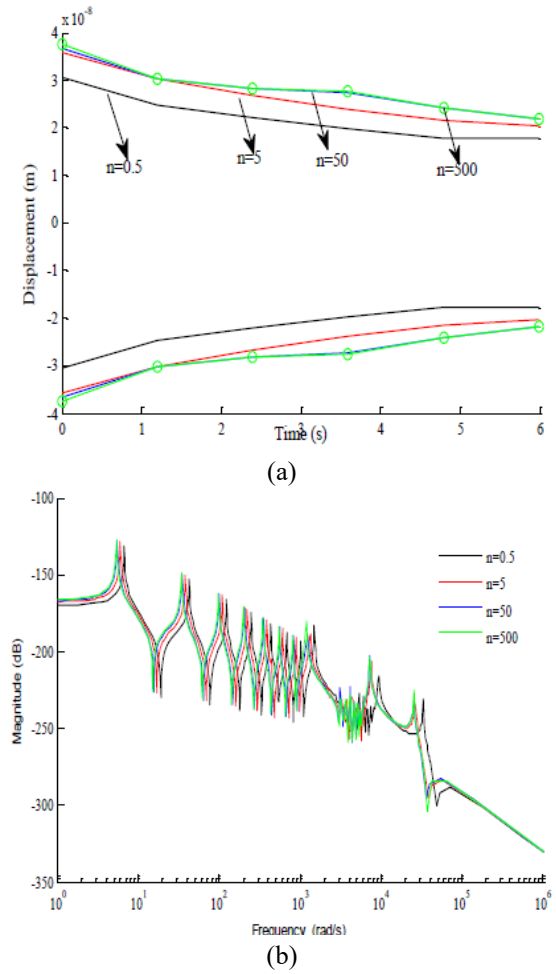


Fig. 4 Envelopes of impulse and frequency responses for FGM beam

unchanged with the increase of volume fraction index  $n$  when volume fraction index  $n$  is large enough. This can be explained that metal plays a dominant role in FGM when volume fraction index  $n$  becomes large enough, and the effective material properties has no obvious changes with the increase of the volume fraction index  $n$  (Xu *et al.* 2016).

Compared to the host FGM beam without piezoelectric layers, the first two normalized mode shapes for the piezoelectric FGM beam are illustrated in Fig. 3(a) and Fig. 3(b), showing the effect of piezoelectric layers on the mode shapes of the host FGM beam. It is seen that the introduction of piezoelectric layers has no significant effect on the mode shapes of the structure.

Fig. 4 give the envelopes of impulses and frequency responses for the FGM beam with different volume fraction indices, from which it is seen that the amplitude of vibration is getting larger (Fig. 4(a)) and the resonant frequency is getting lower with the increase of volume fraction index (Fig. 4(b)), which means the FGM beam becomes more flexible and more susceptible to vibration and may last for a long time.

### 6.2 Active control without considering uncertainties

Considering the more dominant contribution of lower

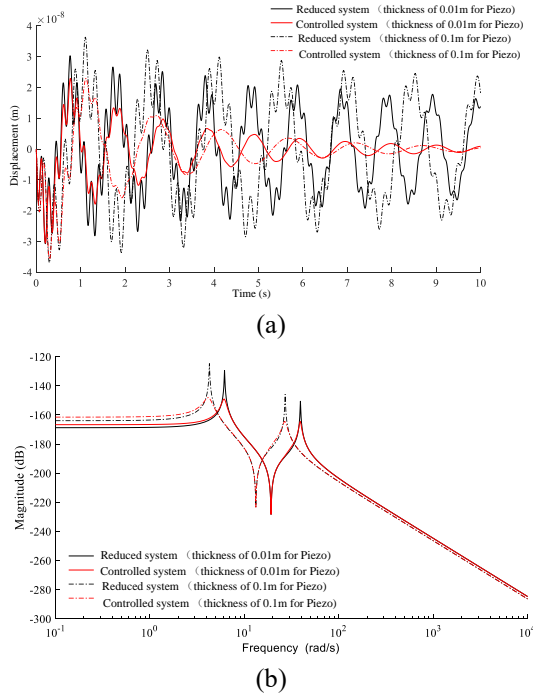


Fig. 5 Impulse and frequency responses for the uncontrolled and controlled reduced systems ( $n=2$ )

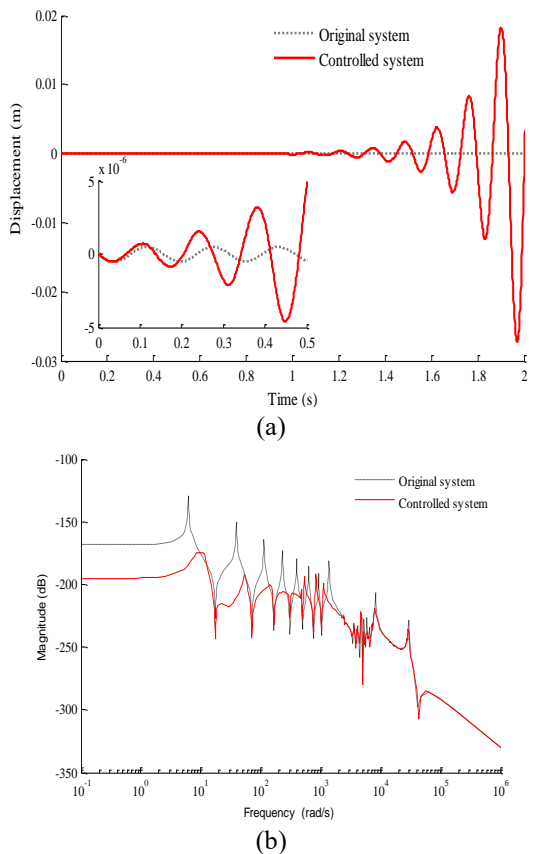


Fig. 6 Impulse and frequency responses for the original and controlled systems ( $n=2$ )

modes to the system response compared to high modes, first two modes are included in the reduce model which is required for the design of implementable output-feedback

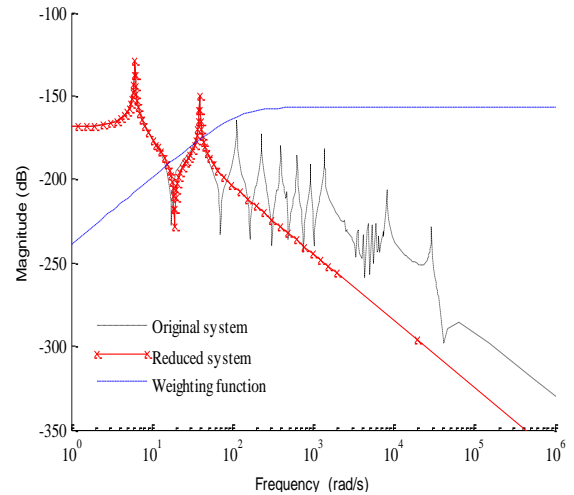


Fig. 7 Frequency responses for the original system, reduced model and weighting function ( $n=2$ )

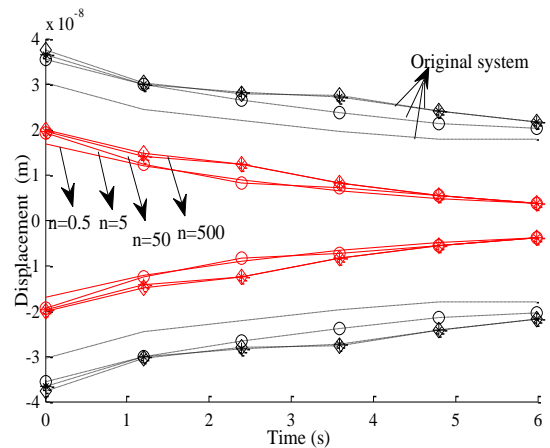


Fig. 8 Envelopes of impulse responses for original and controlled system with different  $n$

H-infinity controller.

Without considering uncertainties, a dynamic output-feedback H-infinity control law based on the reduced model including first two modes is designed. Fig. 5 gives the impulse responses and frequency responses for the uncontrolled and controlled reduced system without considering the uncertainties, from which the first two modes are excellently suppressed. It is also seen that the thickness of piezoelectric layer has obvious effects on the dynamic characteristics and response of structure and has no dominant effects on the control performance since the effect of piezoelectric layer on the host structure has been taken into accounted in the development of structural model used for designing the control law.

However, the problem has arisen when the control law based on the reduced model was applied to the original system. Fig. 6 gives the impulse responses and frequency responses for the uncontrolled original and controlled systems without considering the uncertainties, from which it is evident that some high modes are excited when the low frequencies are controlled (Fig. 6(b)), and the system vibration response cannot be suppressed (Fig. 6(a)).

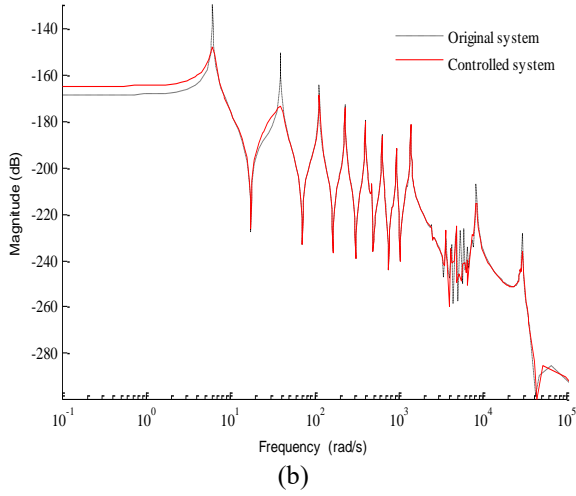
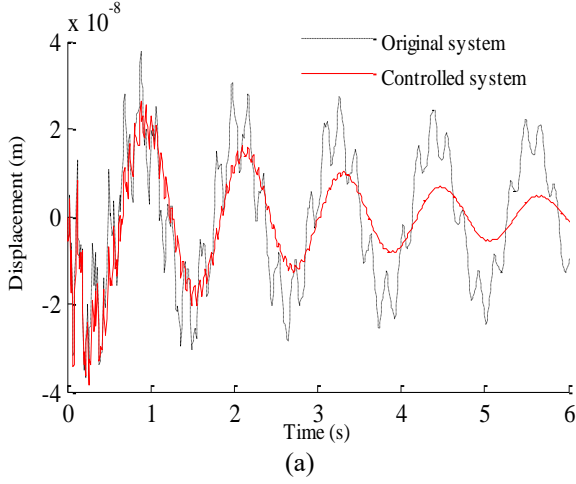


Fig. 9 Impulse and frequency responses for the original and controlled systems ( $n=2$ )

### 6.3 Robust control with considering uncertainties

Considering the uncertainties coming from the parameters and the high modes excluded in the reduced model, an output-feedback H-infinity robust control law is designed in this part. 1% random error in modal parameters is considered. For the modelling error, the following weighting function  $e(s)$  forming the upper bound of the unmodeled high-frequency modes is utilized

$$e(s) = \frac{1e - 8s^2}{s^2 + 2 * 115s + 115^2}, \quad (46)$$

and Fig. 7 gives the frequency responses for the original, reduced model and weighting system.

Applying the control law with considering the uncertainties to the original system, Fig. 8 gives the envelopes of the impulse responses for the uncontrolled and controlled system, from which the proposed control method is effective for different volume fraction indices and the amplitude of vibration is relatively smaller for the smaller volume fraction indices.

Fig. 9 gives the impulse responses and frequency responses for the uncontrolled and controlled system with considering the uncertainties, from which it can be seen that

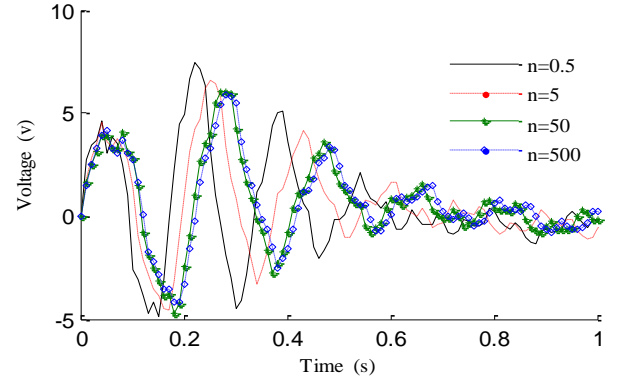


Fig. 10 Control voltages applied to the piezoelectric actuator for different volume fraction indices

the low-frequency modes is suppressed without exciting the high-frequency modes (Fig. 9(b)), and therefore the spillover appearing in the control without considering uncertainties is avoided and the vibration response is suppressed (Fig. 9(a)).

Fig. 10 gives the control voltages applied to the piezoelectric actuator for the controlled system with different volume fraction indices. It is observed that, in the beginning of control process, the control voltage is larger for the smaller volume fraction volume index compared to the larger volume fraction volume index, which means the suppression of vibration for the FGM beam with smaller volume fraction index need more efforts due to the large stiffness.

### 6.4 Comparative study

The experimental studies on active control of FGM structures are extremely scarce in the literature for the complexity in the manufacturing and fabrication process of FGMs and the difficulty of experiment test for the FGM structure. So, for comparative purpose, both the efficient linear quadratic regulator (LQR) (Bruant and Proslieir 2013) and the proposed method are employed to control the vibration of the FGM beam with piezoelectric layers. In LQR method, the control law can be expressed as

$$\Phi_a(t) = -\mathbf{Kz}(t) \quad (47)$$

which minimizes a cost function given by

$$J = \frac{1}{2} \int_0^{\infty} (\mathbf{z}^T(t)\mathbf{Qz}(t) + \Phi_a^T(t)\mathbf{R}\Phi_a(t))dt, \quad (48)$$

$$\mathbf{R} > 0, \mathbf{Q} \geq 0$$

where  $\mathbf{R}$ ,  $\mathbf{Q}$  are the weighting matrices of state variables and input variables respectively and tuned to refine the LQR control law. With the decrease of  $\mathbf{R}$  value or the increase of  $\mathbf{Q}$  value, the better control performance is obtained while higher control cost is required or the higher input voltage is applied to the piezoelectric actuator. The optimal solution is

$$\mathbf{K} = \mathbf{R}^{-1}\mathbf{BP} \quad (49)$$

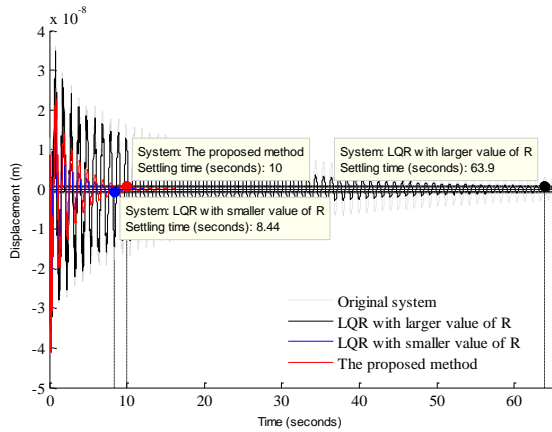


Fig. 11 Impulse responses for the controlled system by using different control methods

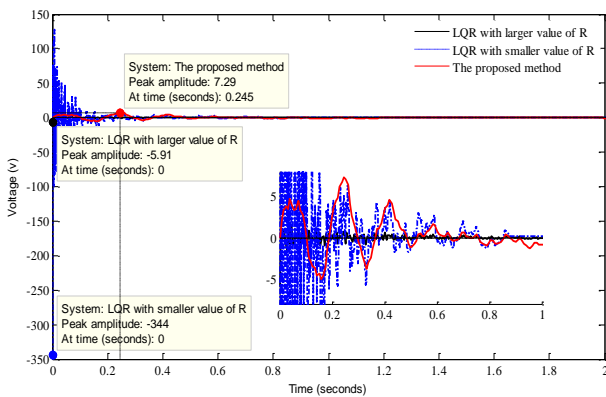


Fig. 12 Control voltages applied to piezoelectric actuator for different control methods

where  $\mathbf{P}$  is the solution of Riccati equation (Schulz and Gomes 2013).

Compared to the LQR method with different values of  $\mathbf{R}$ , the impulse responses for the controlled system by using the proposed control method are shown in the Fig. 11. It is seen that the better time-domain response can be obtained for the controlled systems by using the proposed control method or the LQR method with the smaller value of  $\mathbf{R}$ , having a settling time of 10s for the proposed control method and 8.44 s for the LQR method with smaller value of  $\mathbf{R}$ , respectively, while the time-domain response is not satisfactory for the controlled system by using the LQR method with relatively higher value of  $\mathbf{R}$ , having a settling time of 65 s.

The input voltages applied to the piezoelectric actuator for the proposed control method and the LQR method with different values of  $\mathbf{R}$  are given in Fig. 12. It is observed that, compared to the LQR method with smaller value of  $\mathbf{R}$ , much less input voltage is required to obtain the same control performance in the proposed control method. In the LQR method with smaller value of  $\mathbf{R}$ , the applied input voltages have peaked at 344 V. In the case of the same order of input voltage, the better control performance can be obtained for the proposed control method law than that of LQR method with larger value of  $\mathbf{R}$ .

## 7. Conclusions

The dynamic model has been developed for piezoelectric FGM beams, based on which linear fraction state-space representation for the structure considering both the inherent uncertainties in constitution material properties as well as material distribution and the model error due to mode truncation. Based on which, a dynamic output feedback H-infinity robust control law is designed by using the linear matrix inequality for the purpose of suppressing the vibration of the piezoelectric FGM structure. The following conclusions can be obtained from this study.

(1) Compared to the host structure without piezoelectric layers, the modal frequencies become smaller for the piezoelectric FGM beam. The volume fraction index has a dominant effect on the structural dynamic characteristics and response, in which modal frequencies decrease and the amplitudes of vibration increase with the increase of the volume fraction index.

(2) The higher modes may be excited when the lower modes have been suppressed for the original system by using the control law without considering the uncertainties due to the model reduction.

(3) The vibration of the original system can be controlled by using the control law considering the uncertainties, in which the low frequency modes can be suppressed without exciting the high-frequency modes, and therefore the spillover appearing in the vibration control can be avoided.

(4) Compared to the linear quadratic regulator (LQR), the same control performance for the controlled system can be achieved just by applying less control voltage to the piezoelectric actuator in the proposed control method.

## Acknowledgments

The authors would like to acknowledge financial support of Science Foundation of Shaanxi Province (China) under Grant No. 2016JM1021 and National Science Foundation of China under Grant No.11502183.

## References

- Berardengo, M., Manzoni, S. and Conti, A.M. (2017), "Multi-mode passive piezoelectric shunt damping by means of matrix inequalities", *J. Sound Vibr.*, **405**, 287-305.
- Bodaghi, M., Damanpack, A.R., Aghdam, M.M. and Shakeri, M. (2014), "Geometrically non-linear transient thermo-elastic response of FG beams integrated with a pair of FG piezoelectric sensors", *Comput. Struct.*, **107**, 48-59.
- Bruant, I. and Proslie, L. (2013), "Improved active control of a functionally graded material beam with piezoelectric patches", *J. Vibr. Contr.*, **1**, 1-22.
- Bruant, I. and Proslie, L. (2016), "Optimal location of piezoelectric actuators for active vibration control of thin axially functionally graded beams", *Int. J. Mech. Mater. Des.*, **12**(2), 173-192.
- Chang, X.H., Xiong, J. and Park, H. (2016), "Fuzzy robust dynamic output feedback control of nonlinear systems with linear fractional parametric uncertainties", *Appl. Math. Comput.*, **291**, 213-225.

- Dogan, V. (2014), "Active vibration control of functionally graded plates under random excitation", *J. Intell. Mater. Syst. Struct.*, **1**, 1-15.
- Duc, N.G., Quan, T.Q. and Luat, V.D. (2015), "Nonlinear dynamic analysis and vibration of shear deformable piezoelectric FGM double curved shallow shells under damping-thermo-electro-mechanical loads", *Comput. Struct.*, **125**, 29-40.
- Farnam, A. and Esfanjani, R.M. (2016), "Improved linear matrix inequality approach to stability analysis of linear systems with interval time-varying delays", *J. Comput. Appl. Math.*, **294**, 49-56.
- Hemmatnezhad, M., Ansari, R. and Rahimii, G.H. (2013), "Large-amplitude free vibrations of functionally graded beams by means of a finite element formulation", *Appl. Math. Model.*, **37**(18-19), 8495-8504.
- Huang, X.L. and Shen, H.S. (2006), "Vibration and dynamic response of functionally graded plates with piezoelectric actuators in thermal environments", *J. Sound Vibr.*, **289**(1-2), 25-53.
- Huang, Y. and Li, X.F. (2010), "A new approach for free vibration of axially functionally graded beams with non-uniform cross-section", *J. Sound Vibr.*, **329**(11), 2291-2303.
- Jadhav, P.A. and Bajoria, K.M. (2013), "Free and forced vibration control of piezoelectric FGM plate subjected to electro-mechanical loading", *Smart Mater. Struct.*, **22**(6), 065021-065035.
- Lee, J.W. and Lee, J.Y. (2017), "Free vibration analysis of functionally graded Bernoulli-Euler beams using an exact transfer matrix expression", *Int. J. Mech. Sci.*, **122**, 1-17.
- Li, Z.J. and Adeli, H. (2016), "New discrete-time robust  $H_2/H_\infty$  algorithm for vibration control of smart structures using linear matrix inequalities", *Eng. Appl. Artif. Intel.*, **55**, 47-57.
- Kiani, Y., Sadighi, M. and Eslami, M.R. (2013), "Dynamic analysis and active control of smart doubly curved FGM panels", *Comput. Struct.*, **102**, 205-216.
- Klug, M., Leite, J.S.V. and Silva, F.P.L. (2015), "Fuzzy dynamic output feedback control through nonlinear Takagi-Sugeno models", *Fuzz. Set. Syst.*, **263**, 92-111.
- Koizumi, M. (1993), "Concept of FGM", *Ceram. Trans.*, **34**, 3-10.
- Mohammad, T. and Singh, B.N. (2015), "Stochastic vibration characteristics of finite element modelled functionally gradient plates", *Comput. Struct.*, **130**, 95-106.
- Nguyen-Quang, K., Dang-Trung, H., Ho-Huu, V., Luong-Van, H. and Nguyen-Thoi, T. (2017), "Analysis and control of FGM plates integrated with piezoelectric sensors and actuators using cell-based smoothed discrete shear gap method(CS-DSG3)", *Comput. Struct.*, **165**, 115-129.
- Kitipornchai, S., Yang, J. and Liew, K.M. (2006), "Random vibration of the functionally graded laminates in thermal environments", *Comput. Meth. Appl. M.*, **195**(9-12), 1075-1095.
- Lal, A., Singh, B.N. and Kumar, R. (2007), "Natural frequency of laminated composite plate resting on an elastic foundation with uncertain system properties", *Struct. Eng. Mech.*, **27**(2), 199-222.
- Nie, G.J., Zhong, Z. and Chen, S.P. (2013), "Analytical solution for a functionally graded beam with arbitrary graded material properties", *Compos. Part B-Eng.*, **44**(1), 274-282.
- Pota, H.R. and Alberts, T.E. (1995), "Multivariable transfer functions for a slewing piezoelectric laminate beam", *ASME J. Dyn. Syst.*, **117**(3), 353-359.
- Ray, M.C. and Sachade, H.M. (2006), "Finite element analysis of smart functionally graded plates", *Int. J. Sol. Struct.*, **43**(18-19), 5468-5484.
- Reddy, J.N., Romanoff, J. and Loya, J.A. (2016), "Nonlinear finite element analysis of functionally graded circular plates with modified couple stress theory", *Eur. J. Mech. A-Sol.*, **56**, 92-104.
- Rittenschober, T. and Schlacher, K. (2012), "Observer-based self sensing actuation of piezoelectric structures for robust vibration control", *Automat.*, **48**(6), 1123-1131.
- Sana, S. and Rao, V.S. (2000), "Application of linear matrix inequalities in the control of smart structural systems", *J. Intell. Mater. Syst. Str.*, **11**(4), 321-323.
- Schulz, S.L., Gomes, H.M. and Awruch, A.M. (2013), "Optimal discrete piezoelectric patch allocation on composite structures for vibration control based on GA and modal LQR", *Comput. Struct.*, **128**, 101-115.
- Selim, B.A., Zhang, L.W. and Liew, K.M. (2016), "Active vibration control of FGM plates with piezoelectric layers based on Reddy's higher-order shear deformation theory", *Comput. Struct.*, **155**, 118-134.
- Selim, B.A., Zhang, L.W. and Liew, K.M. (2017), "Active vibration control of CNT-reinforced composite plates with piezoelectric layers based on Reddy's higher-order shear deformation theory", *Comput. Struct.*, **163**, 350-364.
- Shaker, A., Abdelrahman, W., Tawfik, M. and Sadek, E. (2008), "Stochastic finite element analysis of the free vibration of functionally graded material plates", *Comput. Mech.*, **41**(5), 707-714.
- Shegokar, N.L. and Lal, A. (2014), "Stochastic finite element nonlinear free vibration analysis of piezoelectric functionally graded materials beam subjected to thermo-piezoelectric loadings with material uncertainties", *Meccan.*, **49**(5), 1039-1068.
- Shen, H.S. and Wang, H. (2016), "Postbuckling of pressure-loaded FGM doubly curved panels resting on elastic foundations in thermal environments", *Thin Wall. Struct.*, **100**, 124-133.
- Shirazi, A.H.N., Owji, H.R. and Rafeeyan, M. (2011), "Active vibration control of an FGM rectangular plate using fuzzy Logic controllers", *Proc. Eng.*, **14**, 3019-3026.
- Swaminathan, K. and Sangeetha, D.M. (2017), "Thermal analysis of FGM plates-a critical review of various modeling techniques and solution methods", *Comput. Struct.*, **160**, 43-60.
- Wang, Q.S., Shi, D.Y., Liang, Q. and Shi, X.J. (2016), "A unified solution for vibration analysis of functionally graded circular, annular and sector plates with general boundary conditions", *Compos. Part B-Eng.*, **88**, 264-294.
- Wei, C.Z., Park, S.Y. (2017), "Dynamic optimal output feedback control of satellite formation reconfiguration based on an LMI approach", *Aerosp. Sci. Technol.*, **63**, 214-231.
- Wu, C.P. and Liu, Y.C. (2016), "A review of semi-analytical numerical methods for laminated composite and multilayered functionally graded elastic/piezoelectric plates and shells", *Comput. Struct.*, **147**, 1-15.
- Xu, Y.L., Qian, Y., Chen, J.J. and Song, G. (2015), "Stochastic dynamic characteristics of FGM beams with random material properties", *Comput. Struct.*, **133**, 585-594.
- Xu, Y.L., Qian, Y. and Song, G. (2016), "Stochastic finite element method for free vibration characteristics of random FGM beams", *Appl. Math. Model.*, **40**(23-24), 10238-10253.
- Xu, Y.L., Qian, Y., Chen, J.J. and Song, G. (2015), "Modal-based mixed vibration control for uncertain piezoelectric flexible structures", *Struct. Eng. Mech.*, **55**(1), 229-244.